SCALAR AND VECTOR-MESON SU(3)$_F$ DEGENERACY WITHIN UNITARIZED CHIRAL PERTURBATION THEORY*

J.R. Peláez, P. Rabán, J. Ruiz de Elvira

Departamento de Física Teórica and IPARCOS
Universidad Complutense de Madrid, 28040 Madrid, Spain

Received 4 April 2026, accepted 25 May 2026, published online 10 July 2026

In this paper, we present preliminary results of the study of the SU(3) flavor degeneracy of the lightest scalar and vector meson octets. We employ SU(3)$_F$ chiral perturbation theory at next-to-leading order, combined with the Inverse Amplitude Method. We vary quark masses and track the poles associated with the resonances across different Riemann sheets as we approach the SU(3)$_F$ symmetric limit. We find that the poles usually associated with the physical resonances do not become degenerate. Instead, degeneracy is observed for poles located on the Riemann sheet reached by crossing continuously all branch cuts that coalesce in the symmetric limit.

DOI:10.5506/APhysPolBSupp.19.4-A19

1. Introduction

Resonances are fundamental in atomic, nuclear, and particle physics. The mathematically rigorous definition of a resonance is given by the position of the associated complex pole $\sqrt{s_p} = M_{\rm R} - i\Gamma_{\rm R}/2$ that appears in scattering amplitudes, where $M_{\rm R}$ is the mass of the resonance, and $\Gamma_{\rm R}$ is the inverse of its lifetime. For narrow resonances, far from other singularities, Breit–Wigner (BW) shapes provide a fair description of the profiles observed in data. However, those profiles depend on the specific process, due to the presence of other contributions; hence, BW parametrizations are not valid in many cases. In contrast, the position of the pole associated with a resonance is process-independent, and consequently, it is the definition that has been gradually adopted in the «Review of Particle Physics» [1].

Within Quantum Chromodynamics (QCD), quark-flavor symmetry has a key role. Regarding the light sector, SU(3)$_F$ is an approximate symmetry explicitly broken by the masses of the three light quarks u, d, and s, which form a basis for hadron classification. Still, many assignments of physical

* Presented by J.R. Peláez at the Excited QCD 2026 Workshop, Granada, Spain, 8–14 January, 2026.

states into multiplets remain controversial. This happens for light-scalar mesons, customarily assumed to form a nonet below 1 GeV, but with the so-called inverted hierarchy, where, contrary to quark–antiquark expectations, non-strange resonances are heavier than strange ones. In addition, there is an excess of scalars between 1.2 and 1.8 GeV, complicating the identification of the second scalar nonet.

In this paper, we present preliminary results [2], where we rigorously examine the degeneracy of the lightest scalar and vector-meson resonances in the $SU(3)_F$ limit, *i.e.*, the convergence of the associated poles. To do that, we unitarize chiral perturbation theory (ChPT) with the Inverse Amplitude Method (IAM), and follow the poles in different Riemann sheets towards the $SU(3)_F$ limit.

2. Formalism: Inverse Amplitude Method

At low energies, the pseudoscalar $SU(3)_F$ Nambu–Goldstone bosons (NGB), *i.e.*, pions, kaons, and eta, are the relevant hadronic degrees of freedom due to the spontaneous breaking of the chiral symmetry. ChPT gives a systematic and general perturbative expansion of meson–meson scattering amplitudes $T(s) = T_2(s) + T_4(s) + \cdots$ in powers of momenta and quark masses over the chiral scale $4\pi f_0 \approx 1.2\,\text{GeV}$, where f_0 is the LO pion decay constant, and all the quantities are matrices in the channel space. Here, we will consider the first two orders, obtained in [3]. However, ChPT amplitudes only satisfy unitarity order by order, so if we truncate the series, the resulting expansion violates unitarity. The unitarization of the amplitude is necessary to study the resonances produced in meson–meson interactions. The method we will use is the IAM, which reproduces the NLO ChPT expansion, while satisfying unitarity, describing the scattering data reasonably well up to 1.2 GeV, and generating the lightest scalar and vector resonance poles [3, 4]. The only parameters needed are the NLO ChPT renormalized low-energy constants, and therefore, no spurious parameters appear in this formalism. At one loop, it takes the form $T^{\text{IAM}}(s) = T_2(s)(T_2(s) - T_4(s))^{-1}T_2(s)$, which allows us to analytically continue the IAM amplitudes to the complex plane in different Riemann sheets and look for poles. As the NGB masses m_π, m_K, and m_η appear in the amplitudes, both from the Lagrangian and the kinematics, it is straightforward to study the mass dependence of the light scalar and vector-meson poles, as done in [5, 6]. In this work, we study the $SU(3)_F$ limit by continuously decreasing m_K and m_η to the physical m_π.

3. $SU(3)_F$ limit of light vector-meson resonances

We first consider the case of the lightest vector-mesons, *i.e.*, the $\rho(770)$, $K^*(892)$, $\omega(782)$, and $\phi(1020)$. The reason is that they are narrow, well-isolated, and there is general agreement that they form a nonet. It is believed

that the last two are mixtures of singlet and octet states ϕ_1 and ϕ_8. As we work in the isospin-conserving limit with two-body states, we cannot access the singlet, which couples to three pions, but we can study the whole octet. The (antisymmetric) octet partial-wave combinations are

$$t^{(1)}_{1,8_a} = \tfrac{4}{3}t^{(1)}_{1,\pi\pi} + \tfrac{2}{3}t^{(1)}_{1,K\bar{K}} + \tfrac{4\sqrt{2}}{3}t^{(1)}_{1,\pi\pi\to K\bar{K}} \equiv \hat{t}_\rho/\sigma_{\pi\pi}\,, \tag{1}$$

$$t^{(1/2)}_{1,8_a} = t^{(1/2)}_{1,K\pi} + t^{(1/2)}_{1,K\eta} + 2t^{(1/2)}_{1,K\pi\to K\eta} \equiv \hat{t}_{K^*}/\sigma_{K\pi}\,, \quad t^{(0)}_{1,8_a} = 2t^{(0)}_{1,K\bar{K}} \equiv \hat{t}_{\phi_8}/\sigma_{KK}\,, \tag{2}$$

where we label each amplitude by the name of the resonance that dominates it. We have defined hat amplitudes by multiplying by the phase space of the lightest coupled channel. In the left panel of Fig. 1, we show the modulus of these amplitudes in the real axis above the lightest threshold for different m_K/m_π values. At the physical point, $m_K/m_\pi \approx 3.5$, we see the well-known shapes of the $\rho(770)$ and $K^*(892)$, but also that the ϕ_8 appears below the $K\bar{K}$ threshold, as in [7]. As we decrease m_K (and m_η) towards m_π, the three amplitudes get closer until they converge in the SU(3)$_F$ limit, as expected.

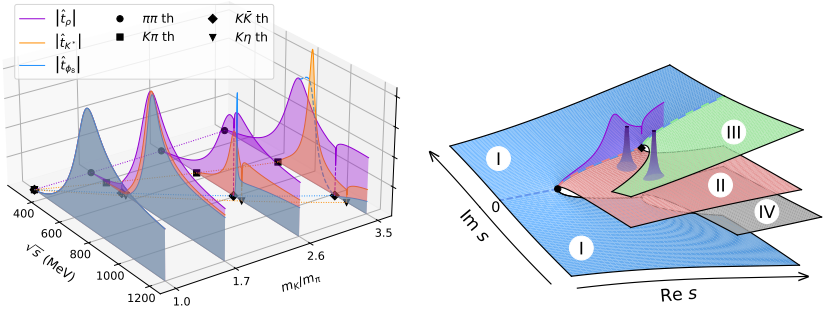

Fig. 1. (Color online) Left: Modulus of the ChPT-IAM amplitudes, on the $\sqrt{s}$ real axis, at several m_K/m_π values, approaching the SU(3)$_F$ limit. Right: Schematic sheet structure for two thresholds, with the physical $|\hat{t}_\rho|$ on the real axis. The first sheet (blue) is continuous with the second (red) in the real axis between the two thresholds, and with the third (green) above the second threshold. Illustrative ρ poles are placed in the second and third sheets. A similar situation holds for the K^*.

Once resonances are identified with their associated poles, we can analyze their degeneracy. Since these poles lie on unphysical Riemann sheets and multiple thresholds are present, it is essential to specify which cuts are crossed continuously, *i.e.*, which sheet is being considered. A generic two-threshold situation is illustrated in the right panel of Fig. 1: the second sheet (shown in red) is reached by crossing the real axis between the two thresholds, while the third sheet (in green) is obtained by crossing above the second branch cut. For reference, we also display the modulus of the $|\hat{t}_\rho|$ amplitude on the real axis in the physical case, together with representative

poles on both unphysical sheets, as realized for the physical ρ or K^*. The second-sheet pole lies much closer to the real axis than the third-sheet one, which justifies neglecting the latter and defining the $\rho(770)$ solely through the second-sheet pole in the physical case. However, as we approach the $SU(3)_F$ limit, this picture changes significantly, as we discuss below.

In Fig. 2, we display the pole trajectories of the ρ and K^* resonances on both Riemann sheets — the second (left panel) and the third (right panel) — as we move from the physical point to the $SU(3)_F$ limit. We use the same color scheme as in Fig. 1 and also include the ϕ_8 trajectory. The poles usually associated with the physical resonances do not converge, contrary to naive expectations. Instead, degeneracy emerges only for poles on the third sheet. From now on, we will call "completely adjacent" sheet, the one reached by crossing all thresholds continuously. This behavior can be understood from the evolution of the thresholds: as the $SU(3)_F$ limit is approached, they move closer together and eventually coincide. As a result, the second sheet for the ρ and K^* becomes disconnected from the real axis, while the third sheet becomes adjacent to the first from the degenerate threshold up to infinity. Therefore, the poles that degenerate in the $SU(3)_F$ limit are those on the completely adjacent sheet. Equivalently, when all thresholds overlap, all cuts must be treated the same; otherwise, the analytic continuation would explicitly break the $SU(3)_F$ symmetry.

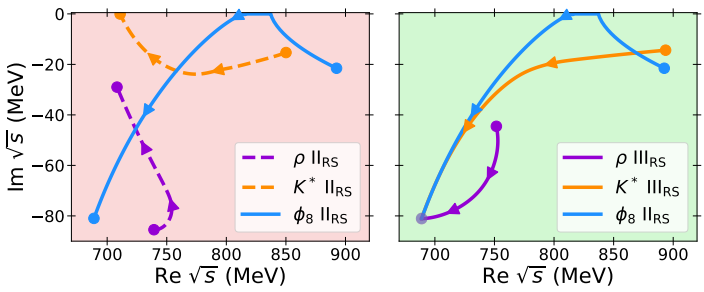

Fig. 2. Light-vector trajectories in the second (left panel) and third (right panel) Riemann sheets, using the ChPT-IAM amplitudes from the physical point to the $SU(3)_F$ limit $m_K, m_\eta \to m_{\pi_{\rm phys}}$. The ϕ_8 trajectory is attached to both panels. The poles from the third sheet are those that converge in the SU(3) limit.

In addition, the widths of the ρ and K^* from the second sheet in the $SU(3)_F$ limit can be understood from Eqs. (1) and (2) with a simple Flatté model, in a similar way as in [8]. The partial decay widths of the resonances to each of the two channels are proportional to the coefficient multiplying the amplitude of that channel, *i.e.*, to the squared coupling. In addition, when the cut of a channel is not crossed continuously, the contribution of

its partial width to the pole position changes its sign. Therefore,

$$\begin{aligned}\frac{\Gamma_\rho^{\mathrm{SU(3)},II}}{\Gamma_\rho^{\mathrm{SU(3)},III}} &= \frac{\Gamma^{\mathrm{SU(3)}}_{\rho\to\pi\pi} - \Gamma^{\mathrm{SU(3)}}_{\rho\to K\bar{K}}}{\Gamma^{\mathrm{SU(3)}}_{\rho\to\pi\pi} + \Gamma^{\mathrm{SU(3)}}_{\rho\to K\bar{K}}} = \frac{4/3-2/3}{4/3+2/3} = \frac{1}{3}\,,\\ \frac{\Gamma_{K^*}^{\mathrm{SU(3)},II}}{\Gamma_{K^*}^{\mathrm{SU(3)},III}} &= \frac{\Gamma^{\mathrm{SU(3)}}_{K^*\to K\pi} - \Gamma^{\mathrm{SU(3)}}_{K^*\to K\eta}}{\Gamma^{\mathrm{SU(3)}}_{K^*\to K\pi} + \Gamma^{\mathrm{SU(3)}}_{K^*\to K\eta}} = \frac{1-1}{1+1} = 0\,,\end{aligned} \tag{3}$$

which approximately explains what we see in Fig. 2.

4. SU(3)$_F$ limit of light scalar-meson resonances

Now, let us briefly discuss the SU(3)$_F$ limit for the lightest scalars. This case is more challenging, as both the octet and singlet sectors are accessible, and the scalar multiplet is significantly more controversial than its vector counterpart. These resonances are the σ, $f_0(980)$, κ, and $a_0(980)$, with the singlet and octet states, f_1 and f_8, mixing to produce the physical σ and $f_0(980)$. This limit was already studied within the leading-order chiral unitary approach in [9]. However, in [9], the poles are followed along the second sheet and then connected to trajectories on the completely adjacent sheet, resulting in paths that are not continuous. Here, instead, we track the poles simultaneously across the relevant Riemann sheets, ensuring a continuous description of their evolution. Our results are shown in Fig. 3.

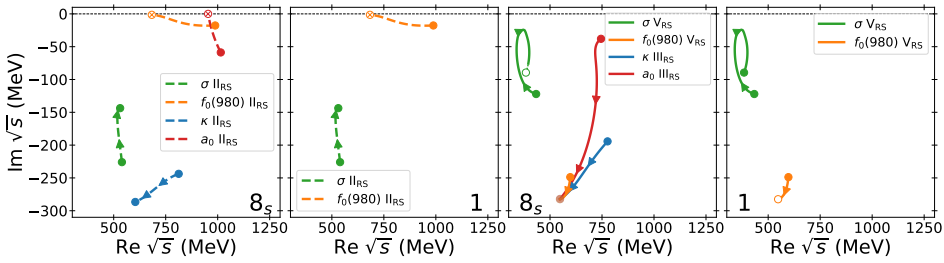

Fig. 3. Light-scalar trajectories using the ChPT-IAM amplitudes from the physical point to the SU(3)$_F$ limit $m_K, m_\eta \to m_{\pi_{\mathrm{phys}}}$. We show results for both the octet and singlet amplitudes in separate panels. The two leftmost panels correspond to the trajectories of the poles that start from the physical poles. The two rightmost panels show the trajectories in the completely adjacent sheet for each resonance.

We get similar conclusions as in the vector sector: the poles usually associated with the physical resonances do not converge in the SU(3)$_F$; instead, the poles from the completely adjacent sheet (fifth for the isoscalar ones, third for κ, and a_0) become degenerate for the same multiplet. This allows

us to confirm that f_8, κ and $a_0(980)$ belong to the same $SU(3)_F$ octet, and that the $f_0(980)$ has a dominant contribution from the f_8. This last result comes from the fact that the $f_0(980)$ disappears from the singlet amplitude close to the $SU(3)_F$ limit (the end of the trajectory in the octet counterpart is marked with an empty marker). Similarly, we conclude that the σ resonance is dominated by the singlet state f_1. The unintuitive features we have described may be relevant for multiplet identification even if a pole is apparently missing: it may not lie in the usual sheet. Also, because two poles in different sheets may be mistakenly associated with two states, while they may correspond to the same one.

5. Summary

We present preliminary results [2], in which we carry out a detailed study of the $SU(3)_F$ degeneracy of the lightest scalar and vector mesons, understood in terms of the convergence of their associated poles. Our analysis is based on ChPT unitarized via the IAM. Contrary to naive expectations, the poles typically associated with these resonances at physical quark masses do not become degenerate in the $SU(3)_F$ limit. Instead, degeneracy is realized only by poles located on the Riemann sheets reached by continuously crossing all two-meson branch cuts. This shows that the dynamical and symmetry-breaking information of a resonance cannot, in general, be encoded in a single pole. This feature appears to be general and should be taken into account when assigning multiplet structures to other hadrons.

This work is funded by the MCIN/AEI/ 10.13039/501100011033 (grant PID2022-136510NB-C31) and the European Union's Horizon 2020 research and innovation program (grant No. 824093). P.R. is supported by the Spanish Ministerio de Universidades, fellowship FPU21/03878, and J.R.E. by the Ramón y Cajal program (RYC2019-027605-I) of the Spanish MICIU.

REFERENCES

[1] S. Navas *et al.*, *Phys. Rev. D* **110**, 030001 (2024).
[2] J.R. Peláez, P. Rabán, J. Ruiz de Elvira, arXiv:2606.14634 [hep-ph].
[3] A. Gomez Nicola, J.R. Pelaez, *Phys. Rev. D* **65**, 054009 (2002).
[4] J.R. Pelaez, *Mod. Phys. Lett. A* **19**, 2879 (2004).
[5] C. Hanhart *et al.*, *Phys. Rev. Lett.* **100**, 152001 (2008).
[6] J. Nebreda, J.R. Pelaez, *Phys. Rev. D* **81**, 054035 (2010).
[7] J.A. Oller, E. Oset, J.R. Pelaez, *Phys. Rev. D* **62**, 114017 (2000).
[8] V. Burkert *et al.*, *Phys. Lett. B* **844**, 138070 (2023).
[9] J.A. Oller, *Nucl. Phys. A* **727**, 353 (2003).